J. Chem. Sci. (2020) 132:144
https://doi.org/10.1007/s12039-020-01848-4

REGULAR ARTICLE

Effect of crystalline phases and acid sites on the dehydration of 1-octadecanol to 1-octadecene over TiO_2–ZrO_2 mixed oxides

TINGMING DUAN[a,b], YONG XIAO[a,*], GUOQUAN ZHANG[a], BO HOU[a], LITAO JIA[a] and DEBAO LI[a]

[a]State Key Laboratory of Coal Conversion, Institute of Coal Chemistry, Chinese Academy of Science, Taiyuan 030001, Shanxi, China
[b]University of Chinese Academy of Sciences, Beijing 100039, China
E-mail: xiaoyong@sxicc.ac.cn

MS received 26 April 2020; revised 11 August 2020; accepted 20 August 2020

Abstract. TiO_2–ZrO_2 mixed oxides with different amounts of TiO_2 were prepared by co-precipitation method and used to synthesize 1-octadecene from 1-octadecanol. The results show that the doping of TiO_2 leads to the formation of Lewis acid sites and Brønsted acid sites on the TiO_2–ZrO_2 mixed oxides. For catalysts with TiO_2 doping < 3 wt.%, the catalysts are in an intermediate state from the monoclinic and tetragonal zirconia crystalline phases to the amorphous form, and no Ti–O–Zr bond is formed. For catalysts with TiO_2 doping ≥ 3 wt.%, an amorphous structure and Ti–O–Zr bond are formed. The crystalline phase of metal oxides, amount and type of acid sites simultaneously affect the performance of the catalysts. The acid sites on TiO_2–ZrO_2 mixed oxides with monoclinic and tetragonal zirconia crystalline phases have much lower dehydration activity than those with an amorphous form. Lewis acid sites are responsible for both the dehydration of 1-octadecanol to form 1-octadecene and the double carbon bond migration of 1-octadecene to form 2-octadecene. Brønsted acid sites mainly catalyze the double carbon bond migration of 1-octadecene.

Keywords. Dehydration reaction; TiO_2–ZrO_2 mixed oxides; Ti–O–Zr bond; Acid sites.

1. Introduction

Linear α-olefins is an important organic raw material, being used in polyolefin comonomers, detergents, synthetic lubricants, etc.[1,2] Dehydration of fatty alcohol is an effective way to convert biomass alcohol (usually C_8–C_{18} alcohol) into linear α-olefins.[3,4] Dehydration catalysts for different alcohols mainly include molecular sieves, CeO_2, Al_2O_3, ZrO_2, TiO_2 and TiO_2–ZrO_2 mixed oxides.[5–16] The catalytic performance of TiO_2–ZrO_2 mixed oxides is higher than that of ZrO_2 or TiO_2 because the interaction of TiO_2 and ZrO_2 leads to an increase in the BET surface area and the amount of acid sites.[17–20]

Manrıquez *et al.*,[15] prepared TiO_2–ZrO_2 mixed oxides catalysts with different TiO_2 content by sol-gel method and used them to catalyze the dehydration reaction of isopropanol. They studied the effect of Lewis acid sites on the dehydration behavior of the catalysts but did not explore the effect of the crystalline phase of the TiO_2–ZrO_2 mixed oxides on the dehydration behavior. Vishwanathan *et al.*,[19] prepared a series of amorphous TiO_2–ZrO_2 mixed oxides by co-precipitation method and applied them to dehydration of methanol to dimethyl ether. The results showed that TiO_2–ZrO_2 mixed oxides catalysts with amorphous form had more acid sites and higher methanol conversion than the catalysts containing monoclinic and tetragonal ZrO_2 crystalline phases. However, the dehydration of methanol to dimethyl ether is an intermolecular dehydration reaction, while the dehydration of fatty alcohol to α-olefins is an intramolecular dehydration reaction. It has been reported that the active sites for intermolecular dehydration of isopropanol were different from those for intramolecular dehydration.[15] Therefore, further research is necessary to confirm whether TiO_2–ZrO_2 mixed oxides with amorphous structure can be applied to the intramolecular dehydration of fatty alcohol.

Also, TiO_2–ZrO_2 mixed oxides used for the intramolecular dehydration reaction reported in the above literature is dehydration of isopropanol to propylene. The process of isopropanol dehydration to

*For correspondence

Published online: 30 October 2020

propylene does not generate internal olefin due to the special molecular structure of propylene containing 3 carbon atoms. However, the process of long-chain fatty alcohol dehydration to 1-olefin includes a side reaction of the conversion of 1-olefin to 2-olefin, which is catalyzed by acid sites different from those catalyzing dehydration of fatty alcohol.[21] It is unclear which active sites on the TiO_2–ZrO_2 mixed oxide catalyzes the conversion of 1-olefin to 2-olefin.

To illustrate the above problem, a series of TiO_2–ZrO_2 mixed oxides with different TiO_2 doping content were prepared by co-precipitation method and applied to the dehydration of 1-octadecanol to 1-octadecene. The effect of crystalline phase of TiO_2–ZrO_2 mixed oxides, amount and type (Lewis or Brønsted) of acid sites on the dehydration of 1-octadecanol to 1-octadecene and the conversion of 1-octadecene to 2-octadecene are focused in this study.

2. Experimental

2.1 *Catalyst preparation*

The TiO_2–ZrO_2 mixed oxides were prepared by the co-precipitation method, using $Ti(SO_4)_2$ (Aladdin $\geq$ 96%) and $ZrOCl_2{\cdot}8H_2O$ (Aladdin 98%) as precursor material. Appropriate amounts of $Ti(SO_4)_2$ solution (0.5 mol/L) and $ZrOCl_2{\cdot}8H_2O$ solution (1.0 mol/L) were mixed and the mixture was added dropwise with the diluted $NH_3{\cdot}H_2O$ (wt = 25%), the pH value of the mixed solution was adjusted to 9 and the solution was aged for 4 h. The precipitate was separated from the mixed solution and purified by deionized water. Then the precipitate was dried in an oven at 110 °C for 12 h and heated to 400 °C at a rate of 1 °C/min for 4 h in a muffle furnace. The catalyst was denoted as xTiO_2–ZrO_2, where x represents the quality of TiO_2 content. The preparation steps of ZrO_2 and TiO_2 were the same as mentioned above.

2.2 *Catalyst characterization*

X-ray Power diffraction (XRD) was measured on a Panalytical X'pert diffractometer using Cu K_α (wavelength λ = 0.154 nm) radiation operated at 40 kV and 40 mA, the spectra were scanned 5° to 90°, and the scanning speed was 2 °C /min.

The texture properties information of the catalyst such as the specific surface area, pore volume and pore size were obtained with a Micromeritics ASAP 2460 analyzer at liquid nitrogen temperature. Before measurements, the samples were degassed at 300 °C for 12 h under vacuum.

Laser Raman spectroscopy was performed using 50 mV air-cooled He-Cd laser with 325 nm on a HJY LabRAM HR800 Raman spectrometer.

The acid sites were measured on the Nicolet Magna 550 infrared adsorption instrument. Prior to measurement, the sample was dried at 110 °C for 12 h. Then 30 mg of the sample was compressed into self-supporting pieces, and placed in an IR cell and treated under vacuum at 300 °C. After cooling down to 120 °C, the catalyst was exposed to pyridine for 30 min. In the process of recording the infrared spectrum of the sample, the infrared spectrum of the air was used as the background. The sample was raised to 250 °C at a rate of 10 °C/min, and the spectrum was collected after 5 min of desorption.

Elemental analysis was determined by Thermo iCAP 7000 inductively coupled plasma emission spectrometer. The 0.1 g sample was dissolved in the mixed acid under heating and stirring conditions to obtain the contents of Ti and Zr, and then the contents of TiO_2 and ZrO_2 were obtained. The data collection was done automatically by the computer.

The surface composition of the catalysts was calculated by an X-ray photoelectron spectrometer (AXIS ULTRA DLD). Al Kα (hν = 1486.6 eV) was used as the excitation source, the C1s peak was employed as an internal standard to revised electric charge effect. The XPS fitting and peak integration were done using XPSPEAK software.

2.3 *Catalyst evaluation*

The performances of the catalysts were carried out in a stainless steel fixed-bed reactor. N_2 was used as the carrier gas, and the raw material (1-octadecanol) and carrier gas flowed through the reactor tube from top to bottom. The size of the reactor filled with the catalyst is 10 mm × 500 mm ($\Phi \times$ L). 4 mL catalyst (20–40 mesh) was loaded in the reactor. There is a steel pipe in the middle of the reactor, and a thermocouple is inserted into the pipe to monitor the temperature of the center of the catalyst. The dehydration reaction of 1-octadecanol was performed at atmospheric pressure, and the carrier gas flow rate was 30 mL/min. After slowly raising the reaction tube to the reaction temperature, a pump was used to feed the liquid into the reactor. The time to reach a steady-state was not less than 24 h. The liquid-phase products were collected in a low-temperature collector (10 °C) and a high-

temperature collector (110 °C), and the products were collected and analyzed every 24 h. The effluent gases were analyzed on GC-950 chromatographs of Shimadzu using a Carbosieve-packed column equipped with a thermal conductivity detector (TCD) and an Al_2O_3 column equipped with a flame ionization detector (FID). Liquid products were dissolved in CS_2, and analyzed offline by Shimadzu GC-2010 chromatography with a 30 m TMX-1 capillary column.

3. Results and Discussion

3.1 *Crystal phase structure of the catalysts*

The XRD spectra of ZrO_2, TiO_2 and TiO_2-ZrO_2 mixed oxides catalysts with different TiO_2 content were shown in Figure 1a. For ZrO_2, there are several obvious diffraction peaks at 24.3°, 28.4°, 31.6° and 34.5° belonging to the monoclinic ZrO_2 crystalline phase (PDF#37-1484) and at 30.2° and 50.4° belonging to the tetragonal ZrO_2 crystalline phase (PDF#42-1164).[22] For TiO_2, the diffraction peaks at 25.2°, 37.6°, 48.1° and 53.7° can be observed, which is assigned to anatase crystalline phase (PDF#21-1272).[23,24] The crystalline phase of 1% TiO_2-ZrO_2 and 2%TiO_2-ZrO_2 are similar to that of pure ZrO_2, which were mainly monoclinic and tetragonal ZrO_2 crystalline phases, but the intensity of the characteristic peaks is gradually weakened. As TiO_2 doping is more than 3 wt.%, each TiO_2–ZrO_2 mixed oxide contains only one broad peak, which indicates that crystalline phase changes to amorphous form. According to calculations, the crystal diameters of ZrO_2, 1%TiO_2–ZrO_2, and 2% TiO_2–ZrO_2 are 7.7 nm, 6.0 nm, and 5.6 nm, respectively. As TiO_2 doping is more than 3 wt.%, the crystal diameter cannot be obtained due to the formation of an amorphous structure.

To further investigate, the interaction between ZrO_2 and TiO_2 were tested by Raman spectrum analysis (-Figure 1b). Raman spectrum for ZrO_2 contains peaks at 178, 270, 336, 476, 634 and 754 cm^{-1}, which are assigned to monoclinic and tetragonal ZrO_2 crystalline phases.[25–27] The Raman spectrum of TiO_2 has no obvious characteristic peaks. Catalysts with TiO_2 doping of 3 wt.%, 10 wt.% and 20 wt.% all show a Raman peak at 786 cm^{-1}, which is a characteristic peak of Ti–O–Zr bond.[28,29] Although no Ti–O–Zr characteristic peak was observed in the catalysts with TiO_2 doping of 1 wt.% and 2 wt.%, the characteristic peaks of the monoclinic and tetragonal ZrO_2 crystalline phases were weakened, which indicates that they are in the intermediate state from the crystalline phase to amorphous form.

3.2 *Texture of the catalysts*

The BET surface area (A_{BET}), pore volume and average pore diameter of TiO_2-ZrO_2 mixed oxides with different TiO_2 content were listed in Table 1. A_{BET} of the catalysts gradually increases with an increase in TiO_2 doping. It is worth noting that, though no amorphous structure forms in 1% TiO_2–ZrO_2 and 2% TiO_2–ZrO_2 (obtained from Figure 1), the doping of TiO_2 significantly increases A_{BET} of the catalysts. This also indicates that 1% TiO_2–ZrO_2 and 2% TiO_2–ZrO_2 were in the intermediate state from monoclinic and tetragonal ZrO_2 crystalline phases to amorphous structure.

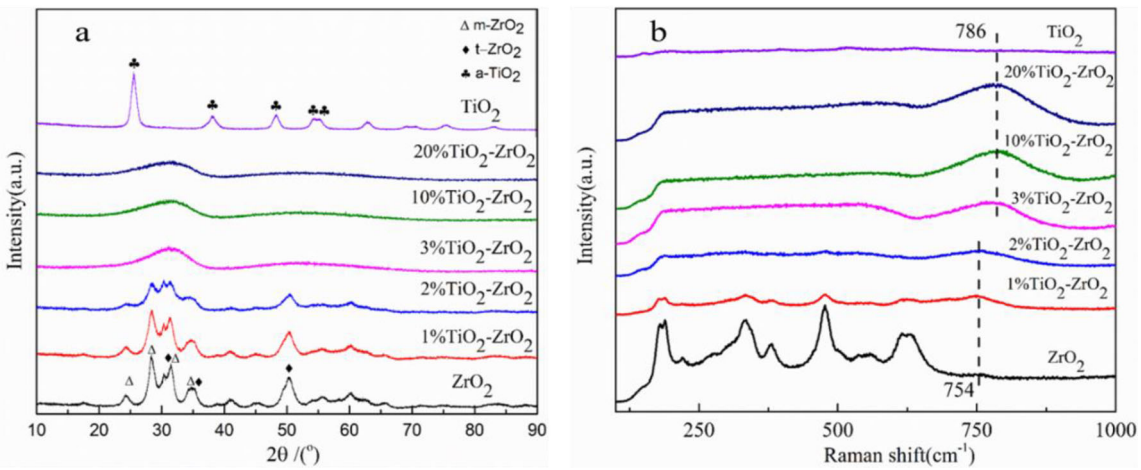

Figure 1. XRD profiles (a) and Raman spectra (b) of the catalysts.

Table 1. Texture parameters of TiO_2-ZrO_2 mixed oxides with different TiO_2 content.

Sample	A_{BET}/(m^2 g^{-1})	Pore volume v/(cm^3 g^{-1})	Average pore diameter d/nm
ZrO_2	1341	0.09	3.2
1%TiO_2–ZrO_2	156	0.12	3.5
2%TiO_2–ZrO_2	185	0.19	4.2
3%TiO_2–ZrO_2	191	0.15	3.5
10%TiO_2–ZrO_2	199	0.19	4.7
20%TiO_2–ZrO_2	240	0.25	5.4
TiO_2	137	0.22	6.4

3.3 *Chemical environmental characterization of metal oxides on catalysts*

X-photoelectron spectroscopy was performed to get more information about the surface composition of the catalysts. The XPS spectra of the catalysts are shown in Figure 2, where Figure 2a and 2b, respectively revealed the Zr 3d and Ti 2p binding energy spectrum. The spin-orbit splitting of Zr is Zr $3d_{5/2}$ and Zr $3d_{3/2}$, and the spin-orbit splitting of Ti is Ti $2p_{3/2}$ and Ti $2p_{1/2}$. Figure 2a shows that for the catalysts with TiO_2 doping <3 wt.%, the values of Zr 3d binding energy are the same as those of pure ZrO_2, for the catalysts with TiO_2 doping ≥ 3 wt.%, Zr 3d binding energy shift to a higher binding energy value, indicating the electron density around Zr decreases. Figure 2b shows that for all the TiO_2–ZrO_2 mixed oxides, Ti 2p binding energy shift to a lower binding energy value, indicating the electron density around Ti increases. The movement of Zr 3d and Ti 2p binding energy further indicates the interaction between Zr and Ti.[30–32] This result is in agreement with that shown in Figure 1b.

Both Raman spectrum and XPS spectrum reveal that intermediate state or amorphous structure forms in TiO_2–ZrO_2 mixed oxides due to the interaction of TiO_2 and ZrO_2. To further clarify whether the mixed oxides composition on the surface and inside of the catalyst is consistent, the peaks in XPS spectrum were integrated and compared with the results obtained by ICP test (Table 2). It shows the $TiO_2/(TiO_2 + ZrO_2)$ value on the surface is higher than that inside, indicating that TiO_2 is enriched on the catalyst surface.

3.4 *Characterization of the surface acid sites of the catalysts*

To clarify the difference in the amount and type of acid sites on the catalyst surface, the samples were subjected to a Pyridine-FTIR test. The spectra are given in Figure 3. No adsorption band is observed for ZrO_2, indicating the amount of acid sites on ZrO_2 are very small. Absorption bands around 1445, 1489 and 1608 cm^{-1} can be observed in 1% TiO_2–ZrO_2, 2% TiO_2–ZrO_2 and 3% TiO_2–ZrO_2. In addition to the above three bands, adsorption bands at 1540 cm^{-1} can be observed in 10%TiO_2–ZrO_2 and 20%TiO_2–ZrO_2. The adsorption bands at 1445 cm^{-1} and 1608 cm^{-1} are identified as Lewis acid, the adsorption band at 1540 cm^{-1} is identified as Brønsted acid, and the band

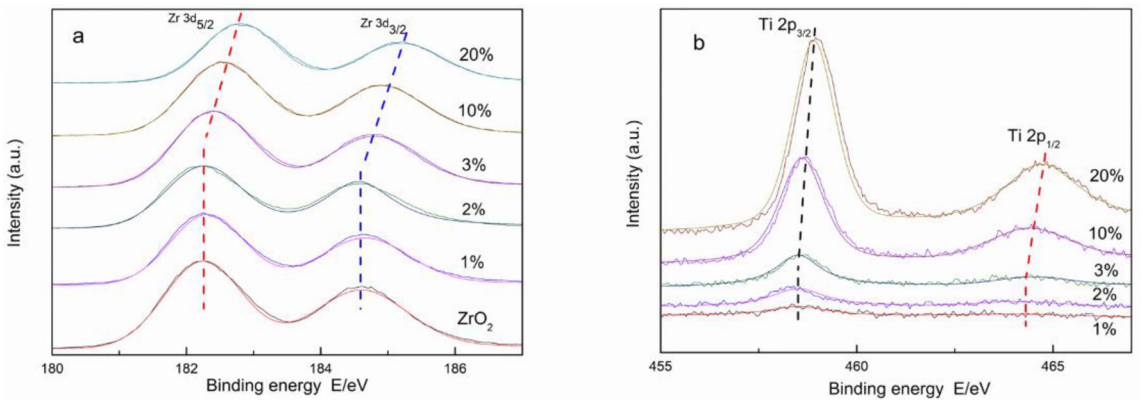

Figure 2. Zr 3d (a) and Ti 2p binding energy spectra (b) of the catalysts.

Table 2. Surface composition of the catalysts.

Catalyst	Binding energy E/eV				$TiO_2/(TiO_2 + ZrO_2)$	
	Zr $3d_{5/2}$	Zr $3d_{3/2}$	Ti $2p_{3/2}$	Ti $2p_{1/2}$	XPS (%)	ICP(%)
1%TiO_2–ZrO_2	182.3	184.6	458.5	464.4	1.34	0.98
2%TiO_2–ZrO_2	182.3	184.6	458.5	464.4	2.25	1.8
3%TiO_2–ZrO_2	182.4	184.8	458.5	464.4	3.35	2.7
10%TiO_2–ZrO_2	182.5	184.9	458.7	464.5	10.14	9.6
20%TiO_2–ZrO_2	182.8	185.2	458.9	464.6	20.15	19.2

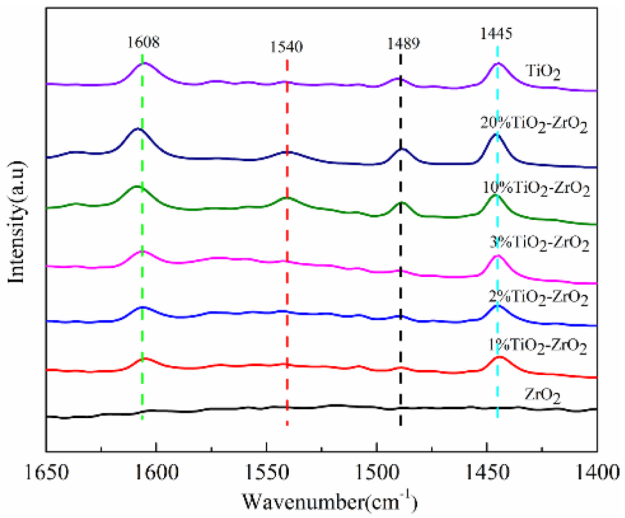

Figure 3. Py-IR spectra of the catalysts.

at 1489 cm^{-1} is assigned to the interaction of Brønsted acid and Lewis acid.[33–35]

The number of Lewis acid and Brønsted acid sites was calculated according to the adsorption band areas in Figure 3, and the results were listed in Table 3. Quantitative calculation of Lewis acid and Brønsted acid is according to the literature.[35,36] The molar extinction coefficients of Lewis acid and Brønsted acid follow the method of literature.[37] The calculated results are: ε (1445) = 1.42 cm μmol^{-1}, ε (1540) = 1.88 cm μmol^{-1}. The table shows that the number of Lewis acid sites in the catalysts gradually increases with an increase in TiO_2 doping, while the Brønsted acid sites is almost absent as the amount of TiO_2 is 1–3 wt.%, and the Brønsted acid sites begin to appear and continue to increase as the amount of TiO_2 reaches 10%.

Table 3. The acid amount of Lewis and Brønsted in the samples.

Catalysts	Acid amount (μmol/g)		
	B	L	Total
1%TiO_2–ZrO_2	–	81	81
2%TiO_2–ZrO_2	–	93	93
3%TiO_2–ZrO_2	–	109	109
10%TiO_2–ZrO_2	31	148	179
20%TiO_2–ZrO_2	41	184	225

3.5 *Catalytic performance of 1-octadecanol dehydration*

The conversion of 1-octadecanol and the selectivity of product over the TiO_2-ZrO_2 oxides were summarized in Table 4. The conversion of 1-octadecanol over ZrO_2 is very low. The conversion of 1-octadecanol gradually increases (except that the value of 2% TiO_2–ZrO_2 is slightly lower than that of 1% TiO_2–ZrO_2) with an increase in TiO_2 doping from 1 to 20 wt.%, increasing from 8.7 to 99.9%. It is worth noting that the conversion of 1-octadecanol sharply increases from 19.8 to 79.2% with an increase in TiO_2 doping from 2 to 3 wt.%. Table 4 also shows that the selectivity of 1-octadecene gradually increases with an increase in TiO_2 doping from 1 to 3 wt.%, but then decreases with a further increase in TiO_2 doping to 20 wt.%. The selectivity of 2-octadecene gradually increases with an increase in TiO_2 doping (except that the value of 2% TiO_2–ZrO_2 is slightly lower than that of 1% TiO_2–ZrO_2).

To illustrate the relationship between the acid sites on the catalyst surface and the activities of the catalysts, the yields of 1-octadecene, 2-octadecene and total octadecene were plotted against the amount of Lewis acid sites on the catalyst surface (Figure 4). For 1%TiO_2–ZrO_2, 2%TiO_2–ZrO_2 and 3%TiO_2–ZrO_2, there are only Lewis acid sites and almost no Brønsted acid sites on catalyst surface, while both 1-octadecene and 2-octadecene were generated during the reaction, as the doping amount of TiO_2 was increased, both the amount of Lewis acid sites and the yield of total

Table 4. Catalytic conversion of 1-octadecanol and product selectivity of the catalysts.

Catalysts	Conversion (%)	Selectivity (%)					
		1-octadecene	Trans-2-octadecene	Cis-2-octadecene	Dioctadecyl ether	Stearaldehyde	Others
ZrO_2	8.7	43.3	4.7	2.2	0.6	4.6	44.5
1%TiO_2–ZrO_2	22.4	44.4	7.7	7.0	6.3	0.5	34.1
2%TiO_2–ZrO_2	19.8	55.8	5.8	5.1	0.4	4.1	28.9
3%TiO_2–ZrO_2	79.2	67.3	12.8	13.5	0.1	0.3	6.5
10%TiO_2–ZrO_2	83.9	61.9	15.3	16.8	2.7	0.2	3.1
20%TiO_2–ZrO_2	99.9	51.5	24.5	18.2	0.0	0.4	5.4

Reaction conditions: Temperature: 300 °C, LHSV: 0.6 h^{-1}, N_2 GHSV: 400 h^{-1}, atmosphere pressure, Others: C1–C17 alkanes and alkenes

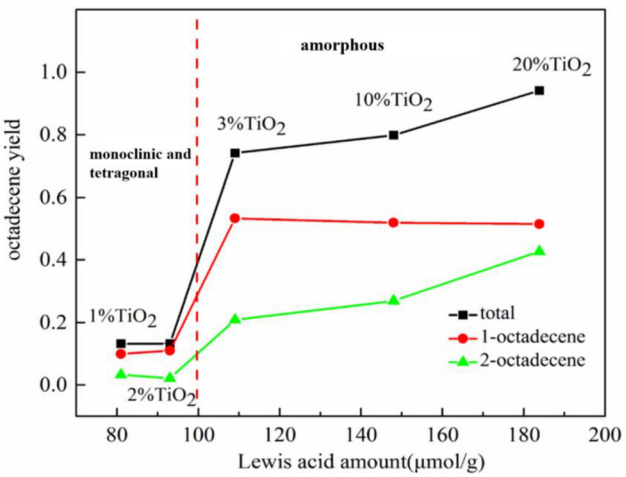

Figure 4. The relationship between the yield of total, 1-octadecene and 2-octadecene and the Lewis acid amount. Total: the sum of 1-octadecene and 2-octadecene; 2-octadecene: the sum of trans-2- octadecene and cis-2-octadecene.

octadecene gradually increase. This indicates that the Lewis acid sites not only catalyze the dehydration of 1-octadecanol to 1-octadecene, but also catalyze the conversion of 1-octadecene to 2-octadecene. With the appearance and increase of Brønsted acid sites on the catalyst, the yield of 1-octadecene gradually decreases but the yield of 2-octadecene gradually increases. The result indicates that Brønsted acid sites mainly catalyze the double carbon bond isomerization, rather than the dehydration of 1-octadecanol to 1-octadecene.

As shown in Figure 4, though there is a certain amount of Lewis acid sites on 1% TiO_2–ZrO_2 and 2% TiO_2–ZrO_2, the yields of 1-octadecene and 2-octadecene are small. As the amount of Lewis acid sites increases, the yields of 1-octadecene and 2-octadecene of 3% TiO_2–ZrO_2 increase sharply, indicating that both the crystalline phase and acid sites affect the performance of the catalyst. Although there is a certain amount of acid sites on 1% TiO_2–ZrO_2 and 2% TiO_2–ZrO_2 with monoclinic and tetragonal ZrO_2 crystalline phases, their contribution to the performance of the catalysts is small. The contribution of the acid sites on 3%TiO_2–ZrO_2, 10%TiO_2–ZrO_2 and 20%TiO_2–ZrO_2 with an amorphous form to the performance of the catalysts increases significantly.

4. Conclusions

With the doping of TiO_2, the formed TiO_2–ZrO_2 mixed oxides gradually change from the monoclinic and tetragonal ZrO_2 crystalline phases to the intermediate state (the amount of TiO_2 is 1 wt% and 2 wt.%). For the TiO_2–ZrO_2 mixed oxides in an intermediate state, the characteristic peaks of the monoclinic and tetragonal ZrO_2 crystalline phases are weakened, but the Ti–O–Zr bond and amorphous structure have not yet appeared. With a continuous increase in TiO_2 doping, the intermediate state changes to an amorphous phase (TiO_2 doping$\geq$ 3 wt%) and Ti–O–Zr bond is formed. Both the formation of the intermediate state and that of amorphous structure lead to a significant increase in A_{BET} and in the amount of acid sites.

The TiO_2–ZrO_2 mixed oxide catalysts show high activity in the dehydration of 1-octadecanol to

1-octadecene. The crystalline phase, amount and type of acid sites comprehensively influence the performance of the catalysts, the acid sites activity on TiO_2–ZrO_2 mixed oxides in the intermediate state is quite low, while that on TiO_2–ZrO_2 mixed oxides in amorphous form increases dramatically. The Lewis acid sites on the TiO_2–ZrO_2 mixed oxides not only catalyze the dehydration of 1-octadecanol to 1-octadecene, but also catalyze the double carbon bond migration of 1-octadecene to form 2-octadecene, the Brønsted acid sites mainly catalyze the double carbon bond migration from the first carbon to the second carbon.

References

1. Echaroj S, Santikunaporn M and Chavadej S 2017 Transformation of bioderived 1-decanol to diesel-like fuel and biobased oil via dehydration and oligomerization reactions *Energy Fuel.* **31** 9465
2. Guo L, Liu W and Chen C 2017 Late transition metal catalyzed α-olefin polymerization and copolymerization with polar monomers *Mater. Chem. Front.* **1** 2487
3. Song W, Liu Y, Barath E, Wang L, Zhao C, Mei D and Lercher J A 2016 Dehydration of 1-octadecanol over H-BEA: a combined experimental and computational study *ACS Catal.* **6** 878
4. Kim Y, Im H B, Jung U H, Park J C, Youn M H, Jeong H D, Lee D W, Rhim G B, Chun D H and Lee K B 2019 Production of linear α-olefin 1-octene via dehydration of 1-octanol over Al_2O_3 catalyst *Fuel* **256** 115957
5. Phung T K, Lagazzo L P, Lagazzo A and Busca G 2015 Dehydration of ethanol over zeolites, silica alumina and alumina: Lewis acidity, Brønsted acidity and confinement effects *Appl. Catal. A-Gen.* **493** 77
6. Kim Y T, Jung K D and Park E D 2010 Gas-phase dehydration of glycerol over ZSM-5 catalysts *Micropor. Mesopor. Mat.* **131** 28
7. Decolatti H P, Dalla B O and Querini C A 2015 Dehydration of glycerol to acrolein using H-ZSM5 zeolite modified by alkali treatment with NaOH *Micropor. Mesopor. Mat.* **204** 180
8. Chokkaram S and Davis B H 1997 Dehydration of 2-octanol over zirconia catalysts: Influence of crystal structure, sulfate addition and pretreatment *J. Mol. Catal. A-Chem.* **118** 89
9. Hong E, Sim H I and Shin C H 2016 The effect of Brønsted acidity of WO_3/ZrO_2 catalysts in dehydration reactions of C3 and C4 alcohols *Chem. Eng. J.* **292** 156
10. Lusvardi V S, Barteau M A and Farneth W E 1995 The effects of bulk titania crystal structure on the adsorption and reaction of aliphatic alcohols *J. Catal.* **153** 41
11. Kostestkyy P, Yu J, Gorte R J and Mpourmpakis G 2014 Structure–activity relationships on metal-oxides: alcohol dehydration *Catal. Sci. Technol.* **4** 3861
12. Gnanamani M K, Jacobs G, Martinelli M, Shafer W D, Hopps S D, Thomas G A and Davis B H 2018 Dehydration of 1,5-Pentanediol over Na-Doped CeO_2 Catalysts *ChemCatChem* **10** 1148
13. Gnanamani M K, Martinelli M, Badoga S, Hopps S D and Davis B H 2018 Dehydration of 1,5-Pentanediol over CeO_2-MeO_x Catalysts *ChemCatChem* **10** 4629
14. Roy S, Mpourmpakis G, Hong D Y, Vlachos D G, Bhan A and Gorte R 2012 Mechanistic study of alcohol dehydration on γ-Al_2O_3 *ACS Catal.* **2** 1846
15. Manrıquez M, López T, Gómez R and Navarrete J 2004 Preparation of TiO_2–ZrO_2 mixed oxides with controlled acid–basic properties *J. Mol. Catal. A-Chem.* **220** 229
16. Duan H, Yamada Y and Sato S 2016 Future prospect of the production of 1, 3-butadiene from butanediols *Chem. Lett.* **45** 1036
17. Li K T, Wang C K, Wang I and Wang C M 2011 Esterification of lactic acid over TiO_2–ZrO_2 catalysts *Appl. Catal. A-Gen.* **392** 180
18. Vishwanathan V, Roh H S, Kim J W and Jun K W 2004 Surface properties and catalytic activity of TiO_2-ZrO_2 mixed oxides in dehydration of methanol to dimethyl ether *Catal. Lett.* **96** 23
19. Li K T, Wang I and Wu J C 2012 Surface and Catalytic Properties of TiO_2–ZrO_2 Mixed Oxides *Catal. Surv. Asia* **16** 240
20. Hirashima Y, Nishiwaki K, Miyakoshi A, Tsuiki H, Ueno A and Nakabayashi H 1988 Role of Ti–O–Zr Bonding in TiO_2–ZrO_2 Catalyst for Dehydrogenation of Ethylbenzene *Bull. Chem. Soc. Jpn.* **61** 1945
21. Berteau P, Delmon B, Dallons J L and Gysel A V 1991 Acid-base properties of silica-aluminas: use of 1-butanol dehydration as a test reaction *Appl. Catal.* **70** 307
22. Chang S and Doong R 2004 The effect of chemical states of dopants on the microstructures and band gaps of metal-doped ZrO_2 thin films at different temperatures *J. Phys. Chem. B* **108** 18098
23. Kundu S, Ciston J, Senanayake S D, Arena D A, Fujita E, Stacchiola D, Barrio L, Navarro R M, Fierro J L and Rodriguez J A 2012 Exploring the structural and electronic properties of Pt/ceria-modified TiO_2 and its photocatalytic activity for water splitting under visible light *J. Phys. Chem. C* **116** 14062
24. Gołąbiewska A, Lisowski W, Jarek M, Nowaczyk G, Michalska M, Jurga S and Medynska A Z 2017 The effect of metals content on the photocatalytic activity of TiO_2 modified by Pt/Au bimetallic nanoparticles prepared by sol-gel method *Mol. Catal.* **442** 154
25. Powers D and Gray H B 1973 Characterization of the thermal dehydration of zirconium oxide halide octahydrates *Inorg. Chem.* **12** 2721
26. Kilo M, Schild C, Wokaun A and Baiker A 1992 Surface oxidic phases of binary and ternary zirconia-supported metal catalysts investigated by Raman spectroscopy *J. Chem. Soc., Faraday Trans.* **88** 1453
27. Miciukiewicz J, Mang T and Knözinger H 1995 Raman spectroscopy characterization of molybdena supported on titania-zirconia mixed oxide *Appl. Catal. A-Gen.* **122** 151
28. Reddy B M, Sreekanth P M, Yamada Y, Xu Q and Kobayashi T 2002 Surface characterization of sulfate, molybdate, and tungstate promoted TiO_2-ZrO_2 solid acid catalysts by XPS and other techniques *Appl. Catal. A-Gen.* **228** 269
29. Kong L, Karatchevtseva I, Zhu H, Qin M J and Aly Z 2019 Synthesis and microstructure characterization of

tetragonal $Zr_{1-x}Ti_xO_2$ (x = 0–1) solid solutions *J. Mater. Sci. Technol*. **35** 1966
30. Reddy B M, Chowdhury B and Smirniotis P G 2001 An XPS study of the dispersion of MoO_3 on TiO_2–ZrO_2, TiO_2–SiO_2, TiO_2–Al_2O_3, SiO_2–ZrO_2, and SiO_2–TiO_2–ZrO_2 mixed oxides *Appl. Catal. A-Gen.* **211** 19
31. Mullins W and Averbach B 1988 Bias-reference X-Ray photoelectron spectroscopy of sapphire and yttrium aluminum garnet crystals *Surf. Sci.* **206** 29
32. Stephenson D and Binkowski N 1976 X-ray photoelectron spectroscopy of silica in theory and experiment *J. Non-Cryst. Solids* **22** 399
33. Barthos R, Lonyi F, Engelhardt J and Valyon J 2000 A study of the acidic and catalytic properties of pure and sulfated zirconia–titania and zirconia–silica mixed oxides *Top. Catal.* **10** 79
34. Gott T and Oyama S T 2009 A general method for determining the role of spectroscopically observed species in reaction mechanisms: Analysis of coverage transients (ACT) *J. Catal.* **263** 359
35. Hong E, Baek S W, Shin M, Suh Y W and Shin C H 2017 Effect of aging temperature during refluxing on the textural and surface acidic properties of zirconia catalysts *J. Ind. Eng. Chem.* **54** 137
36. Emeis C A 1993 Determination of Integrated Molar Extinction Coefficients for Infrared Absorption Bands of Pyridine Adsorbed on Solid Acid Catalysts *J. Catal*. **141** 347
37. Shamzhy J P M, Zhang J, Ruaux V, El-Siblani H and Mintova S 2020 Quantification of Lewis acid sites in 3D and 2D TS-1 zeolites: FTIR spectroscopic study *Catal. Today* **345** 80